GRADUATION THESIS

THE INTERNALIZATION OF APTAMERS IN DENDRITIC CELLS, MODULATING ANTIGEN PRESENTATION

Author: Phuong Thanh Nguyen
Student number: 614299

HAN UNIVERSITY OF APPLIED SCIENCES
LIFE AND MEDICAL SCIENCES INSTITUTE

Table of Contents

List of Abbreviations

APCs	Antigen presenting cells
DAPI	4’,6-diamidino-2-phenylindole
DCs	Dendritic cells
DNA	Deoxynucleotide
DPBS	Dulbecco's phosphate-buffered saline
DTT	Dithiothreitol
ER	Endoplasmic reticulum
FDA	US Food and Drug Administration
HFIP	1,1,1,3,3,3-hexafluor-2-propanol
HIV	Human Immunodeficiency Virus
GM-CSF	Granulocyte-monocyte colony-stimulating Factor
LB	Latex beads
LC-MS	Liquid chromatography-mass spectrometry
LSM	Laser Scanning Microscope
MHC class I	Major Histocompatibility Complex class I
MHC class II	Major Histocompatibility Complex class II
MR	Mannose receptor
MWU	Man-Whitney-U
ODN	Oligodeoxynucleotides
OVA	Ovalbumin
PCR	Polymerase Chain Reaction
PFA	Paraformaldehyde
RNA	Ribonucleotide
RP HPLC	Reverse Phase High Performance Liquid Chromatography
RT	Room temperature
RT-PCR	Reverse Transcription Polymerase Chain Reaction
SELEX	Systematic Evolution of Ligands by Exponential Enrichment
ssDNA	Single-stranded deoxynucleotide
TAP proteins	Transporter associated with antigen processing proteins
TCR	T-cell receptor
TEA	Triethyl amine
TEAA	Triethylammonium acetate
THI-ODN	Thiol-modified oligodeoxynucleotides
VEGF	Vascular endothelial growth factor

1. Abstract

Owing to the non-toxic, nonimmunogenic effects and high affinity to specific molecules, some single-stranded oligonucleotides, namely aptamers, can be exploited in biochemical applications to deliver bioactive elements and interact with the desired targets. Among many identified aptamers, D#7 was utilized to transport antigens to dendritic cells (DCs) by binding selectively to this antigen-presenting cell. After internalization, it lead to the recruitment of further immune responses including activating T cells. However, the pathway how D#7 was processed inside DCs remained unknown. Therefore, this research examined the colocalization of labelled D#7 with ATTO 647N fluorophore and its conjugate to OT-I, a sequence of ovalbumin protein (OVA) consisting of specific binding sequence to Major Histocompatibility Complex (MHC) molecules class I. The positioning of the aptamers over time was investigated in early endosomes, late endosomes and lysosomes at multiple timepoints. Interestingly, D#7 colocalized in three organelles at the same rate at 10 minutes. At 1 hour, the colocalization was more significant in early endosomes. Meanwhile, the conjugate (D#7-OT-I) located predominantly in early endosomes at 10 minutes of internalization. After degradation, the remaining signals shifted mainly to late endosomes at 1 hour. The difference between D#7 and D#7-OT-I confirmed the influence of the antigen on the movements of the aptamers inside DCs. This result highlights the potential of D#7 as a transporter to escort the antigens of interest to DCs selectively, hence, leading to the activation of either cytotoxic T cells or T helper cells.

Keywords: colocalization, aptamers, dendritic cells, T cells, early endosomes, late endosomes, lysosomes

2. Introduction

Aptamers are short chains of single-stranded oligonucleotides, which could be either deoxynucleotides (DNA) or ribonucleotides (RNA), folding into specific secondary and tertiary structures. The length of these oligonucleotides usually varies between 20 to 100 bases [1]. In general, aptamers have a strong specificity for many target molecules including proteins and whole cells. They bind to their targets with high affinity via physiochemical interactions including electrostatic bonding, hydrogen bonds and Van der Waals forces[1]. New aptamers are efficiently generated by a technique called Systematic Evolution of Ligands by Exponential Enrichment (SELEX) from a random oligonucleotide library. The principle of this procedure is based on the selection of oligonucleotides demonstrating specific binding to targets of interest, which are then separated and amplified by Polymerase Chain Reaction (PCR) method in iterative selection rounds. Afterwards, the most promising candidates, which have substantial PCR products, are further characterized and modified depending on the research purpose (Figure 1) [1]. Importantly, some aptamers can persist for a long time *in vivo* (multiple hours to several days) and show nontoxic as well as nonimmunogenic effects, causing almost no harms to the recipients. Due to these special properties, aptamers have been deployed for multiple therapeutics to treat molecular impairments such as cancers, autoimmune or immunosuppressive diseases and bacterial or viral infection [2][3][4][5].

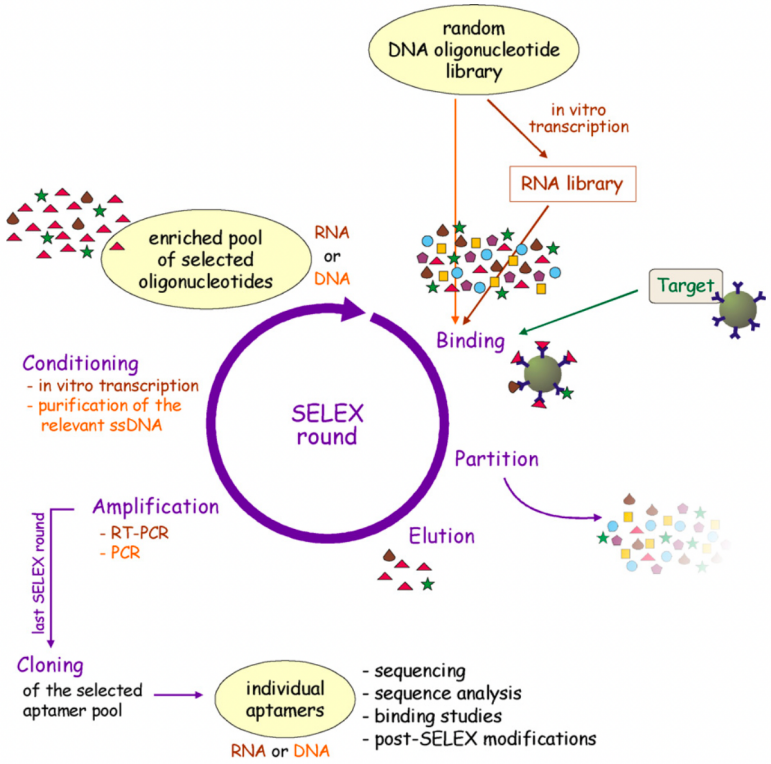

Figure 1: SELEX method to generate pools of aptamers against specific targets [1]. Random DNA or RNA oligonucleotide library are used as the input of SELEX method. The binding targets of aptamers can be inorganic molecules, organic materials such as proteins and complicated structures including whole cells [1]. In the case of D#7 aptamer, dendritic cells were used as the target of selection. During the selection, all the unbound oligonucleotides are washed away. Meanwhile, the sequences binding to targets with high affinity remain bound and can be eluted afterwards. After collecting the sequences of interest, DNA oligonucleotides undergo PCR. In case of RNA oligonucleotide library, the sequences are treated with reverse transcriptase to become ssDNA and amplified [1]. Hence, the amount of these oligonucleotides is enriched. After a few selection rounds by SELEX, the size of the original library is reduced. Only the most enriched sequences are selected for further characterization. They can be used later for sequencing and modification to become aptamers applied in later research.

The key effect of these oligonucleotides thanks to the interactions with their targets. When binding to the protein of interest, these single-stranded nucleotides interfere with protein interactions and probably block the activities of the molecules [4]. Additionally, the aptamers can also resemble the structures of activating ligands, inducing the activities of certain enzymes[6]. The first application of aptamers approved by US Food and Drug Administration (FDA) for macular degeneration was to target Vascular Endothelial Growth Factor (VEGF), diminishing the development of the excessive blood vessels and defective vessels in the eyes. Hence, aptamer therapy manipulates the symptoms of this age-related dysfunction. Furthermore, many aptamers have been tested clinically for future treatments of hematology, oncology, ocular and inflammatory issues [2].

Owing to the specific binding to transmembrane proteins such as receptors, aptamers can also be utilized to transport cargoes to the intracellular compartments [3][4][7]. This property highlights a potential application of drug delivery by aptamers. Aptamers have raised the attention of scientists worldwide to the application of aptamers in vaccination by targeting DCs. These cells are the well-known antigen presenting cells (APCs), functioning to form a link between the innate and adaptive immune systems. By capturing the antigens, DCs process them and present them on Major Histocompatibility Complex (MHC) class I and II, modulating the activation of either $CD4^+$ or $CD8^+$ T cells [8][9].

The mechanisms of internalization in dendritic cells vary including clathrin-, caveolae-mediated endocytosis, and phagocytosis [3][7]. The uptake of antigens by different pathways and mediated receptors determines their fates inside DCs for further processing to prime either $CD8^+$ or $CD4^+$ T cells [7][10]. As an example, mannose receptors (MR) have been found to direct the antigen processing and presentation to $CD8^+$ T cells on MHC class I molecules [11]. After internalizing in early endosomes, the antigens are translocated to the cytosol. Then, the proteasome in the cytoplasm degrades these molecules. The output of which is then transported by transporter associated with antigen processing (TAP) proteins to rough endoplasmic reticulum (ER) and modified to enter the vesicles with MHC class I (Figure 2) [10]. This processing and presentation of antigens on MHC class I is known as cross-presentation in APCs. Meanwhile, DEC205 receptors, recognizing carbohydrate residues on antigens, regulate the processing and presentation of antigens on MHC class II. Hence, antigen presentation leads to priming naive $CD4^+$ T cells [12]. This pathway directs the internalization of antigen-receptor complex in early endosomes (pH 5.5-6). They gradually become late endosomes (pH 5.0-5.5), which are then fused with lysosomes (pH 4.5-5.0) for the breakdown of the bound molecules by lysosomal proteases (Figure 2) [10][13].

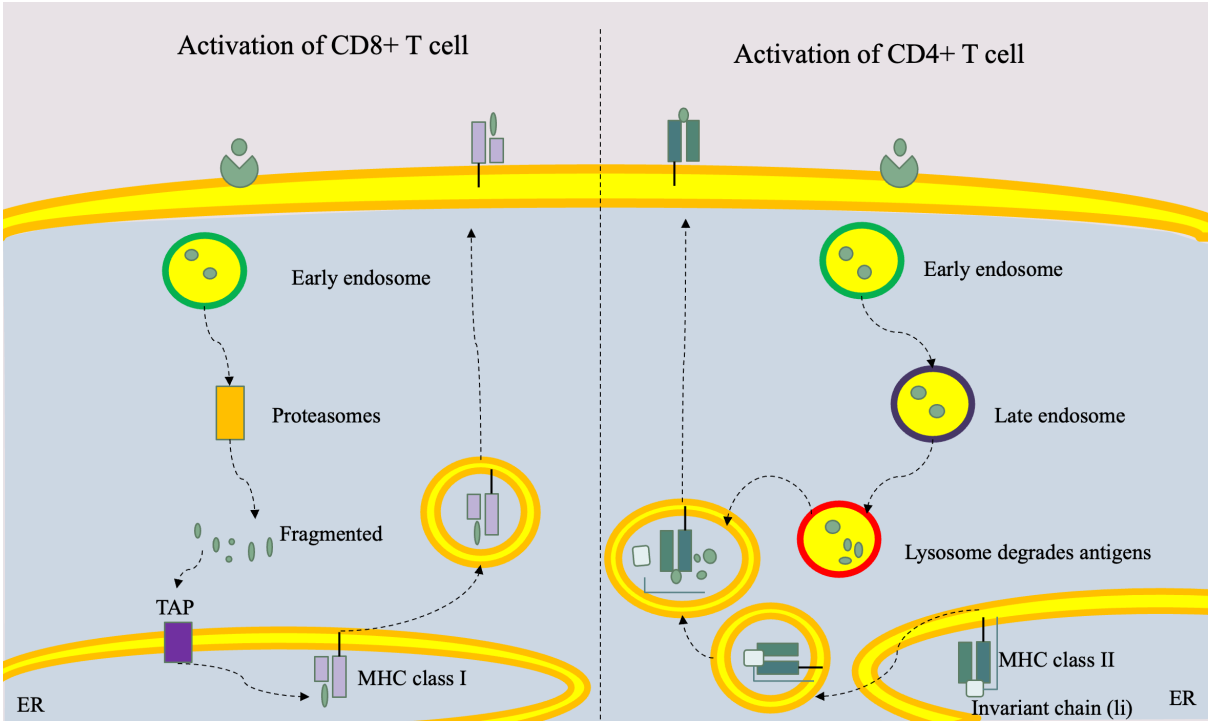

Figure 2: Schematic pathways of the antigen processing and presentation on MHC molecules in DCs. For the activation of $CD8^+$ T cells, the antigen-receptor complex is internalized, which is then broken down by proteasomes in the cytosol. The resulting peptides are transported to ER via TAP proteins. Here, the peptides are bound by MHC class I via the specific recognition regions. ER membrane buds to form a vesicle, transporting the antigen-MHC complex to the surface of DCs. Afterwards, MHC class I on DCs presents the antigen to $CD8^+$ T cells. To activate $CD4^+$ T cells, the antigen-receptor complex is first internalized in early endosome. The vesicle becomes late endosome with the change of pH, which is later fused with lysosomes in DCs. The antigens are cleaved by lysosomal proteases. The cleaved antigens bind to MHC class II after invariant chain (li) leaves MHC class II. The antigen-MHC class II complex is transported in a vesicle to be presented on the surface of DCs. After TCR of $CD4^+$ T cell binds to the presented complex, T cell is activated for further immune activities [13][10].

Upon activation by cross-presentation by APCs, $CD8^+$ T cells gain cytotoxic capacity, inducing apoptosis in target cells such as virus-infected or cancer cells presenting MHC class I-antigen complex on the surface. Meanwhile, activated $CD4^+$ T cells by APCs modulate the differentiation of B cells into plasma cells, producing antibodies against specific pathogens or foreign factors. Additionally, upon activation by antigen uptake, DCs are able to secrete multiple cytokines and growth factors, attracting more immune responses in the body [11][8]. Hence, targeting DCs by antigen-conjugated aptamers is a potential application in vaccine production although this concept is still new and not completely developed in research. Some studies have indicated that the use of aptamers for vaccine development instead of antibodies targeting specific antigens, a commonly used method in vaccination, is more stable and cost-effective [14]. Besides, aptamers can be synthesized *in vitro* [14][15]. More importantly, this technique provides specific binding of molecules of interest, minimizing off-target problems [14].

According to the research of Dr. Haßel [11], some aptamers were identified to target DCs by cell-SELEX methods (Figure 1). There were multiple promising oligonucleotides detected in this process, including D#7 aptamer. D#7 aptamer was shown to bind selectively to DCs instead of B cells or T cells, which is a good transporter candidate for further vaccine development [11]. However, it is unknown to which receptors this aptamer binds on DCs. As discussed above, the pathway resulting in the activation of T cells depends on the mechanisms as well as receptors internalized with the antigens. Hence, it remains uncertain how D#7 aptamer is processed and where this aptamer locates inside DCs. According to the findings of Dr. Haßel, D#7 was shown to colocalize with early endosomes after 10 minutes of incubation

[11]. Meanwhile, very weak colocalization between D#7 aptamer and lysosomes was observed. More importantly, the conjugation between D#7 and OT-I peptide was found to activate cytotoxic T cells. OT-I peptide, also called OVA $_{249-273}$, is a short sequence of commonly known OVA protein. It contains the specific binding sequence to MHC class I, leading to the activation of $CD8^+$ T cells after being presented on the surface of DCs. The activation of cytotoxic T cells was found after 72 hours of incubation with DCs treated with the conjugates [11]. As the follow-up research, the internalization of D#7 aptamers and its conjugate with OT-I was further investigated and described in this thesis.

This research was done to answer two main questions. First, the pathway of the aptamers without the antigens, which remains unknown so far, needs to be observed carefully for better understanding. Secondly, it is questionable if the antigens have an impact on the route of conjugates inside DCs, which might differ from the general pathway of D#7 alone. To investigate this procedure, colocalization analysis at multiple timepoints before 72 hours by the Laser Scanning Microscope (LSM) was utilized.

Specifically, the internalization of the aptamers was closely observed in early endosomes, late endosomes and lysosomes with the appropriate markers attached to the membranes of these compartments. The free aptamers and conjugates were both labelled with ATTO 647N fluorophores. Meanwhile, the cellular compartments were visualized by Alexa Fluor 488 which stained specific markers on the organelles. Particularly, early endosomes could be recognized by EEA1 proteins, an early endosomal Rab5 effector protein, on the membrane of the compartments [16]. In addition, LAMP-1, a lysosomal membrane proteins [17], was deployed to label lysosomes with the fluorophores. To visualize late endosomes, Rab7, a late-endosome-associated GTPase [18], was used as the marker.

Because D#7-OT-I could activate cytotoxic T cells, the pathway of this conjugate was expected to involve early endosomes and the degradation in the cytosol, showing high colocalization with EEA1 on early endosomes. Consequently, the peptides can be presented on MHC class I. Importantly, the route of D#7 alone might differ from the conjugate because the peptides possibly have an impact on the location of D#7 inside DCs.

3. Materials and methods

3.1. Formation of aptamer conjugation by thiol-maleimide coupling

Table 1: Sequences of all the peptides and aptamers involved in this research

Peptides/ aptamers	Sequences
OT-I	
OT-Isc	
MHC-class-I epitope of OT-I	
5'thiol-D#7-3'ATTO 647N (80 bases)	
5'thiol-ctrl-3'ATTO 647 (79 bases)	

As mentioned above, OT-I was used as the antigen conjugated with the aptamers. To compare the results, OT-Isc was used as a negative control. While OT-I contains the binding sequence to MHC class I, OT-Isc does not have this region (Table 1). Maleimide-modified peptides, termed as mal-peptides, (PSL Peptide Specialty Laboratories GmbH) were the input of thiol-maleimide coupling.

The aptamers such as D#7 function as the transporters of the antigens to DCs. There were two aptamers deployed in this research including D#7 and ctrl (Ella Biotech GmbH). Ctrl functions as the non-binding control in this experiment. Table 1 shows the sequences of all the used aptamers and peptides. The aptamers were modified at both ends. The 3' end was attached to

ATTO 647N fluorophore while the 5' end was modified with thiol, which interacted with mal-peptides to form the conjugation.

1M Triethylammonium acetate (TEAA) buffer (Sigma Aldrich) was adjusted to pH 8.3 – 8.5 by triethyl amine (TEA, Fluka). 400µl of each reaction contained 20µl of 100µM oligodeoxynucleotide (ODN) and 40µl of 100mM dithiothreitol (DTT, Roth) in TEAA buffer. The reaction was carried out at 70°C for 3 minutes and incubated at room temperature (RT) for 1 hour.

The sample was purified with Amicon Ultra-0.5 Centrifugal Filter Devices 10K (Milipore), the column of which was first pre-equilibrated with 400µl miliQ water for 15 minutes. In the meantime, the column was centrifuged at 14,000 x g, 4 °C. The sample was added to the column, which was then centrifuged at 14,000 x g, 4°C for 15 minutes. The eluate was discarded. The column was then washed with 400µl miliQ water, and centrifuged at 14,000 x g, 4°C for 15 minutes. The washing step was repeated 4 times. The conjugated aptamers were collected by inverting the column in a new Eppendorf tube, and centrifuged at 1,000 x g, 4°C for 2 minutes. The resulting eluate contained about 40-50µl solution of the conjugates.

80nmol Mal-peptide (dissolved in DPBS, pH 7.0-7.5) was added to 2nmol reduced ODN. The reaction was incubated at RT for 1-2 hours and preserved overnight at 4°C. The conjugated aptamers were purified by Reverse Phase High Performance Liquid Chromatography (RP-HPLC).

3.2. Purification by Reverse Phase High Performance Liquid Chromatography (RP-HPLC)

To separate the conjugated aptamers from free ODN and peptides, HPLC 1260 series, C18 Eclipse column (Agilent) was used. The mobile phase was 10 mM TEA/100 mM 1,1,1,3,3,3-hexafluoro-2-propanol (HFIP, Roth) in miliQ water, filtered through a 0.20µm filter. The column was first flushed with 80% acetonitrile (Fluka). Then, the mobile phase was gradually added to the column. The sample was then pumped into the column gradually with 10µl injections. Along with the mobile phase, acetonitrile was added to the column at increasing rates over time. At a certain concentration of acetonitrile, the conjugated aptamers left the column and were eluted. The retention time indicated by light absorption at 260nm was recorded. Eluted pure conjugates were collected in 2ml Eppendorf tubes in the fraction of a collector tray. The procedure ended with consecutive blank runs to wash the column. Eventually, the mobile phase was changed to 80% acetonitrile to re-equilibrate the column.

The collected sample fractions were placed in the speed vacuum (Thermo Fischer Scientific) at 151mBar, RT to evaporate all the corrosive HFIP for 2 hours. Afterwards, the fractions were snap-frozen in liquid nitrogen. The sample was then freeze-dried overnight at 0.37mBar, -80°C in a Freeze-drier (Christ LCG) to evaporate all the liquid. The precipitates in the collected fractions were resuspended in 400µl of Dulbecco's phosphate-buffered saline (DPBS, Gibco). To collect and concentrate the samples again, the samples were pooled into one 10K Amicon Ultra 0.5 column (Amicon Centrifugal Filter Devices, Milipore). The steps were done similarly to section 4.1 above. However, DPBS was used instead of miliQ water to pre-equilibrate and wash the column. The final output was measured with Nanodrop 2000c Spectrophotometer (Thermo Fischer Scientific) to determine the concentration of the yielded aptamers.

3.3. Immunostaining of DCs for LSM analysis

To have DCs as the input of immunostaining, the bone marrow was isolated from the wildtype mice (C57BL/6J) provided by LIMES Institute. After flushed by PBS, the cells were cultivated in DC-medium for 7 days. The medium contained IMDM medium (Pan Biotech), 10% fetal

bovine serum (Pan Biotech), 2.5% Granulocyte-monocyte colony-stimulating Factor (GM-CSF) from Burgdorf group at LIMES Institute, 100U/ml penicillin-streptomycin (Thermo Fischer Scientific) and 50µM β-mercaptoethanol (Roth). Afterwards, 2 x 10^5 DCs from 7-day cell culture was seeded in 1ml medium per well on a 15mm coverslip in a 4-well plate. The cells were left to adhere to the slip for at least 45 minutes at 37°C. The supernatant was removed, and the wells were washed with 500µl sterile DPBS to remove unbound or dead cells. 200µl medium containing 100nM conjugated aptamers was added to the cells, which were then incubated at 37°C. The kinetics of the vesicles transporting the conjugates was investigated at three timepoints including 10 minutes, 30 minutes and 60 minutes. However, for the free aptamers such as ATTO 647N-ctrl and ATTO 647N-D#7. For the timepoints longer than 10 minutes, the old medium with the conjugates was removed. After that, 1ml DC-medium was added to the wells for longer incubation. The plates were kept in 37°C until the desired timepoints.

Following each step of immunostaining, the cells were washed thoroughly twice or thrice with 1ml DPBS to remove all the previous reagents. The cells in each well were fixated in 200µl of 3.7% paraformaldehyde (PFA, Fluka) in DPBS for 20 minutes at RT. 500µl of 0.1% triton X-100 (Merck) in DPBS for 5 minutes at RT to permeabilize the cells. 500µl of 10% milk powder (Roth) in DPBS was added to the well plates to block non-specific bindings of the antibodies for 1 hour at RT.

The cells were stained with 200µl of primary antibody (1:100 dilution) in DPBS for 45 minutes at RT. For the detection of the early endosomes, Chicken EEA1 antibody (H-300, Santa Cruz) was used. Rat LAMP-1 antibody (1D4B, BD) labelled the lysosomes. Mouse Anti-Rab7 antibody (B-3, Santa Cruz) was utilized to stain the late endosomes. Then, the cells were incubated in 200µl of the secondary antibody (AlexaFluor488, 1:400 dilution) in DPBS for 45 minutes at RT. The used secondary antibodies were anti-rabbit, anti-rat and anti-mouse (Thermo Fischer Scientific). The nuclei were stained with 200µl of 4',6-diamidino-2-phenylindole (DAPI, 1:1000 dilution, Sigma Aldrich) in DPBS for 5 minutes at RT. 1ml MiliQ water was added to each well. The coverslips with attached cells were mounted on slides with Fluorogel Mounting (EMS) and left overnight at RT. The slides were then sealed with the nail polish and stored at 4°C in the dark.

There were some negative controls such as the cells without the internalization of conjugates to select the intensity of fluorescence for each cellular compartment during image observation with LSM. To examine autofluorescence, cells with only DAPI staining were prepared. In addition, cells without primary antibodies were used to check the specificity of the secondary antibodies.

3.4. Colocalization analysis with LSM

The kinetics study was observed with Laser Scanning Microscope 710 (Zeiss) for the colocalization of conjugated aptamers and the organelles of interest such as early endosomes, lysosomes and late endosomes at different timepoints. The images were taken at multiple Z-stacks, allowing 3D imaging of the cells. The Z-stack was taken every 0.24Å in depth of the cells. The colocalization analysis was done by ImageJ with thresholding and median filter to get rid of the background signals [19]. JACoB plugin [19] was used to analyze the colocalization. Colocalization was evaluated by Pearson's correlation coefficient (PCC). While PCC=1 indicates perfectly linear correlation between two signals, PCC=0 shows no correlation. For 0<PCC<1, the correlation is interpreted from a weak to strong correlation [20]. The procedure for image processing and analysis was described in detail in Appendix 1. Macro coding was

written to automate the procedure for all images (Appendix 2). At least 20 cells were collected for each image at one time point for statistical analysis.

3.5. Data analysis

The data of each aptamer and conjugate were calculated for the averages and standard deviations through time to show the kinetics of the colocalization in DCs. Besides, each experimental group was checked for normal distribution by the Shapiro-Wilk test [21] and processed to exclude outliers by boxplots. If the data were normally distributed, one-tailed Student-T tests were done while one-tailed Man-Whitney-U (MWU) tests were used for abnormally distributed data. The p-value < 0.05 was chosen to check the significant differences between two groups of samples. To check if the peptides had an impact on the pathway, statistical test was done between ATTO 647N-D#7 and ATTO 647N-D#7-OT-I. Additionally, to check if the pathway is specific to the activation of CD8+ T cells by SIINFEKL-MHC-class-I complex, the kinetics of ATTO 647N-D#7-OT-I and ATTO 647N-D#7-OT-Isc was statistically compared. Furthermore, the comparison between the colocalizations of the aptamers in early endosomes and in other cellular compartments at the same timepoints were also checked for the significant difference. Python 3.2.9 was utilized for data processing and statistical analysis between different experimental groups was done using Pinguoin package.

4. Results

4.1. HPLC and yield of coupling reactions

Coupling by maleimide-thiol reactions was the first step to generate the conjugates of interest including ctrl-OT-I, D#7-OT-I and D#7-OT-Isc by using ATTO 647N-labelled aptamers. The coupling products were used as the input of HPLC purification to separate the desired conjugates from the unreactive aptamers and free peptides . Figure 3 shows the retention time of the elutes along the timeline. The higher the peaks in mAU, the more conjugates were formed after coupling reactions. The low peaks at around 8.6-8.8 minutes indicate the free aptamers while the highest peak in each chromatogram performs the conjugates of interest. ATTO 647N-ctrl-OT-I was eluted at 9.730 minutes. Meanwhile, ATTO 647N-D#7-OT-I left the column at around 9.853 minutes and the peak of ATTO 647N-D#7-OT-Isc occurred at 9.274 minutes. The peptides were eluted later than 10 minutes. The longer the elements stayed on the column, the more hydrophobic they were. Besides, the peaks of peptides were not narrow nor single peaks. Instead, they showed multiple shoulders, indicating fragmented peptides. There were multiple background peaks before 7 minutes and after 17 minutes, which were also found in the blank.

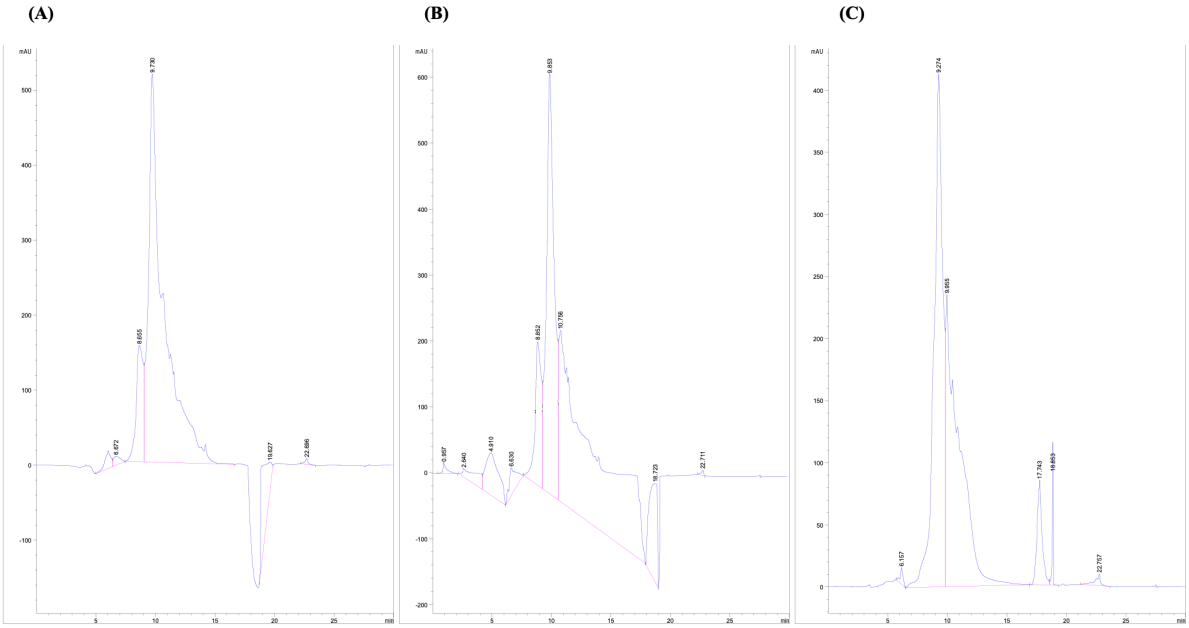

Figure 3: Retention time of the conjugates determined by RP-HPLC. Each chromatogram illustrates the absorbance (mAU) of the eluate at 260nm and the timeline at which the peaks occur. (A) Retention time of ATTO 647N-ctrl-OT-I at 9.730 minutes. (B) Retention time of ATTO 647N-D#7-OT-I at 9.853 minutes. (C) Retention time of ATTO 647N-D#7-OT-Isc at 9.274 minutes. The chromatogram indicates the retention time of the conjugates. Free aptamers were eluted at around 8.6 minutes for ATTO 647N-ctrl and 8.8 minutes for ATTO 647N-D#7 while the peptides left the column at approximately 10 minutes. The highest peak of each chromatogram shows the retention time of the conjugates between aptamers and the peptides (OT-I and OT-Isc). There were multiple peaks after 10 minutes, indicating fragmented peptides. Additionally, there were many background peaks before 7 minutes and after 17 minutes.

After purification, the conjugates were dissolved in DPBS. Unexpectedly, the conjugates had difficulty dissolving in 400µl DPBS. After washing with Amicon column, the conjugates were completely dissolved in around 40-50µl DPBS. Then the final products were determined for quantity and calculated for the final yield (Table 2). The yields of three conjugates were very low in general. Among the three conjugates, ATTO 647N-D#7-OT-I was the lowest, which was less than 10%. ATTO 647N-ctrl-OT-I had the highest yield of more than 25%.

Table 2: The yield of conjugation after purification by HPLC

Name of conjugates	Input of the aptamers (pmol)	Output of the conjugates (pmol)	Yield (%)
ATTO 647N-ctrl-OT-I	2000	535.5	26.77
ATTO 647N-D#7-OT-I	2000	198.15	9.91
ATTO 647N-D#7-OT-Isc	1800	207.4	11.50

4.2. Immunostaining

The internalization of the aptamers and conjugates was investigated in DCs with LSM. ATTO 647N-D#7-OT-I and ATTO 647N-D#7-OT-Isc were incubated with DCs for kinetics study for 10 minutes, 30 minutes and 1 hour. Additionally, ATTO 647N-D#7 was internalized in DCs for 10 minutes, 30 minutes, 1 hour and 2 hours. To compare with the target conjugates, ATTO 647N-ctrl-OT-I was used as the negative control. During the experiments, the images of ATTO 647N-D#7-OT-Isc with Alexa488-anti-EEA1 at 1 hour and Alexa488-anti-Rab7 at 10 minutes failed to be collected.

The internalization of ATTO 647N-ctrl-OT-I in DCs was observed with the LSM. As a comparison, the intensity of this control was much less than the actual samples such as ATTO 647N-D#7-OT-I and ATTO 647N-D#7-OT-Isc. When compared with the conjugates, the intensity of internalized ATTO 647N-ctrl was much less than ATTO 647N-D#7 and ATTO 647N-ctrl-OT-I. Only a few DCs internalized ATTO 647N-ctrl in the kinetics study (results

not shown). Importantly, the negative control with only DAPI showed autofluorescence in the green channels. In addition, the samples without the primary antibodies indicated non-specific binding of the secondary antibodies, leading to background noise of Alexa Fluor 488 signals.

EEA1 on early endosomes were labelled with Alexa Fluor 488, which were shown as granular vesicles inside DCs (Figure 4). Meanwhile, lysosomes were seen more like clouds of green signals by Alexa488-anti-LAMP-1 (Figure 6). Alexa488-anti-Rab7 showed the patterns of both granular and cloudy signals, depending on the cells and the Z stack (Figure 5). Possible colocalization could be seen when overlaying the red channels of ATTO 647N-labelled conjugates and green channels of the organelles. The bright field shows the edges of the cells, indicating irregular shapes of DCs with protrusions.

In general, the signals of ATTO 647N fluorophores were the strongest at 10 minutes of internalization into cells. Over longer time, the signals became weaker and scattered throughout DCs. Clear colocalization between the conjugates and early endosomes at 10 minutes and 30 minutes could be seen in Figure 4, indicated by the white arrows.

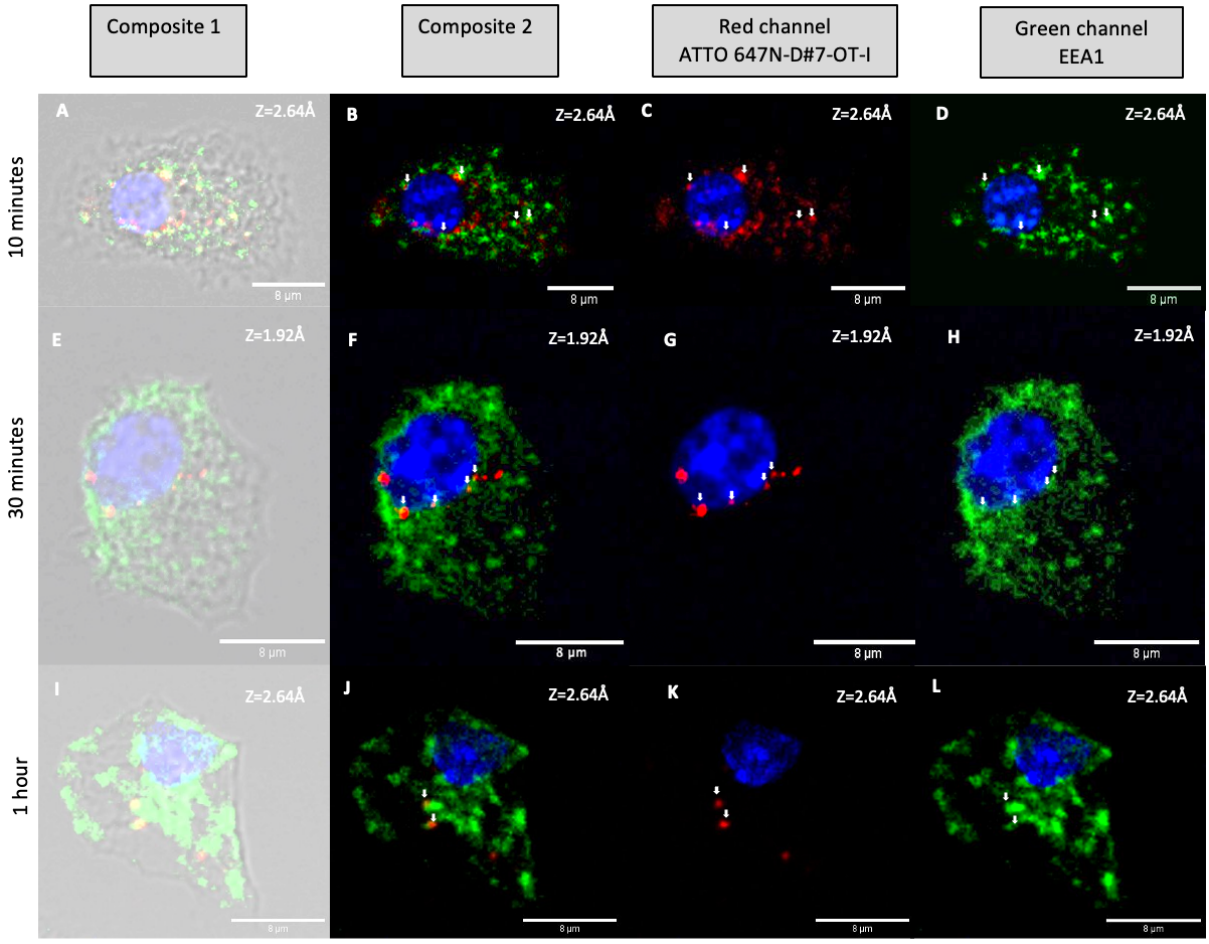

Figure 4: Immunostaining of DCs internalized with ATTO 647N-D#7-OT-I (red signals) at three timepoints and Alexa Fluor 488 (green signals) to label EEA1 on early endosomes. The picture depicts three timepoints at 10 minutes, 30 minutes and 1 hour. Composite 1 comprises all channels with bright field showing the borders of the cells. Composite 2 excludes bright field, illustrating the green and red channels together. DAPI (blue) indicates the nucleus of the cell. Possible colocalizations between ATTO 647N labels and Alexa Fluor 488 are marked by white arrows in Composite 2, Red and Green channels. Each image is performed with a scale bar (8µm) and Z stack (Å). (A) Bright field at 10 minutes. (B) Composite at 10 minutes. (C) Red channel of ATTO 647N label at 10 minutes. (D) Green channel of Alexa488-anti-EEA1 at 10 minutes. (E) Bright field at 30 minutes. (F) Composite at 30 minutes. (G) Red channel of ATTO 647N label at 30 minutes. (H) Green channel of Alexa488-anti-EEA1 at 30 minutes. (I) Bright field at 1 hour. (J) Composite at 1 hour. (K) Red channel of ATTO 647N label at 1 hour. (L) Green channel of Alexa488-anti-EEA1 at 1 hour. The signals of Alexa488-anti-EEA1 were obtained as granular particles inside the cells. The intensity of ATTO 647N-labelled conjugates was reduced at later timepoints, especially at 1 hour. Significant colocalization was seen at 10 and 30 minutes.

Additionally, the possible colocalization was significantly seen with Alexa488-anti-Rab7 on late endosomes at 10 minutes (Figure 5). Meanwhile, the conjugates located less in late endosomes at 30 minutes and 1 hour (images E-L in Figure 5).

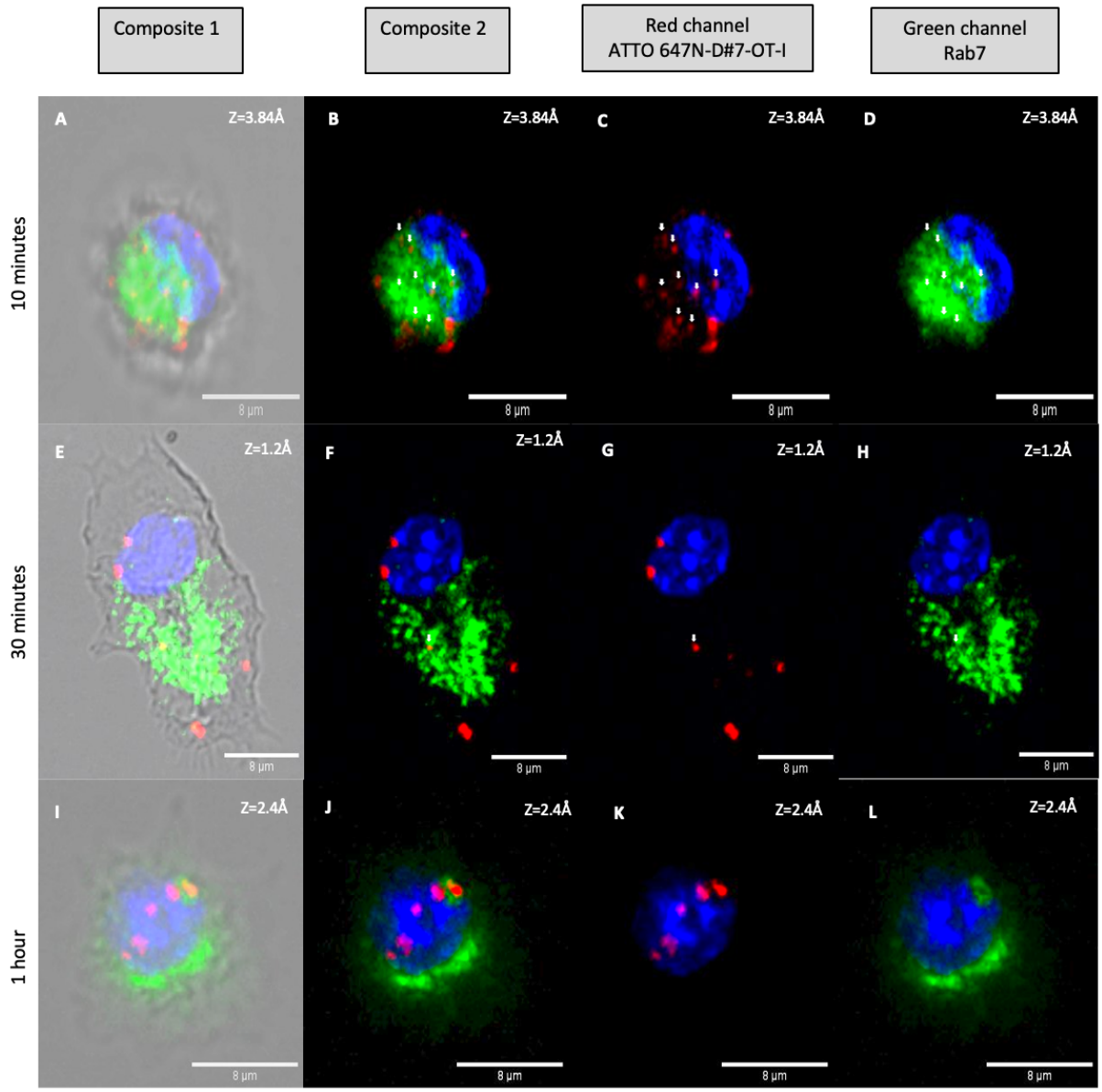

Figure 5: Immunostaining of DCs internalized with ATTO 647N-D#7-OT-I (red signals) at three timepoints and Alexa Fluor 488 (green signals) to label Rab7 on late endosomes. The picture depicts three timepoints at 10 minutes, 30 minutes and 1 hour. Composite 1 comprises all channels with bright field showing the borders of the cells. Composite 2 excludes bright field, illustrating the green and red channels together. DAPI (blue) indicates the nucleus of the cell. Possible colocalizations between ATTO 647N labels and Alexa Fluor 488 are marked by white arrows in Composite 2, Red and Green channels. Each image is performed with a scale bar (8µm) and Z stack (Å). (A) Bright field at 10 minutes. (B) Composite at 10 minutes. (C) Red channel of ATTO 647N label at 10 minutes. (D) Green channel of Alexa488-anti-Rab7 at 10 minutes. (E) Bright field at 30 minutes. (F) Composite at 30 minutes. (G) Red channel of ATTO 647N label at 30 minutes. (H) Green channel of Alexa488-anti-Rab7 at 30 minutes. (I) Bright field at 1 hour. (J) Composite at 1 hour. (K) Red channel of ATTO 647N label at 1 hour. (L) Green channel of Alexa488-anti-Rab7 at 1 hour. Red signals of ATTO 647N-labelled conjugates decreased over time. There was a strong correlation between red and green signals at 10 minutes while the colocalization was insignificant at 30 minutes and 1 hour. The staining of Alexa488-anti-Rab7 was visualized as granular particles or a big cloud of green signals depending on cells and the Z stacks.

Similar patterns were visualized with LAMP-1 on lysosomes in Figure 6. The colocalization in lysosomes after 10 minutes was very weak because the red signals scattered predominantly in the edges of the cells while lysosomes tended to center the cells.

The signals of internalized ATTO 647N-D#7-OT-Isc were the same as the conjugates in the three organelles. There was no difference detected between ATTO 647N-D#7-OT-I and ATTO 647N-D#7-OT-Isc (results not shown).

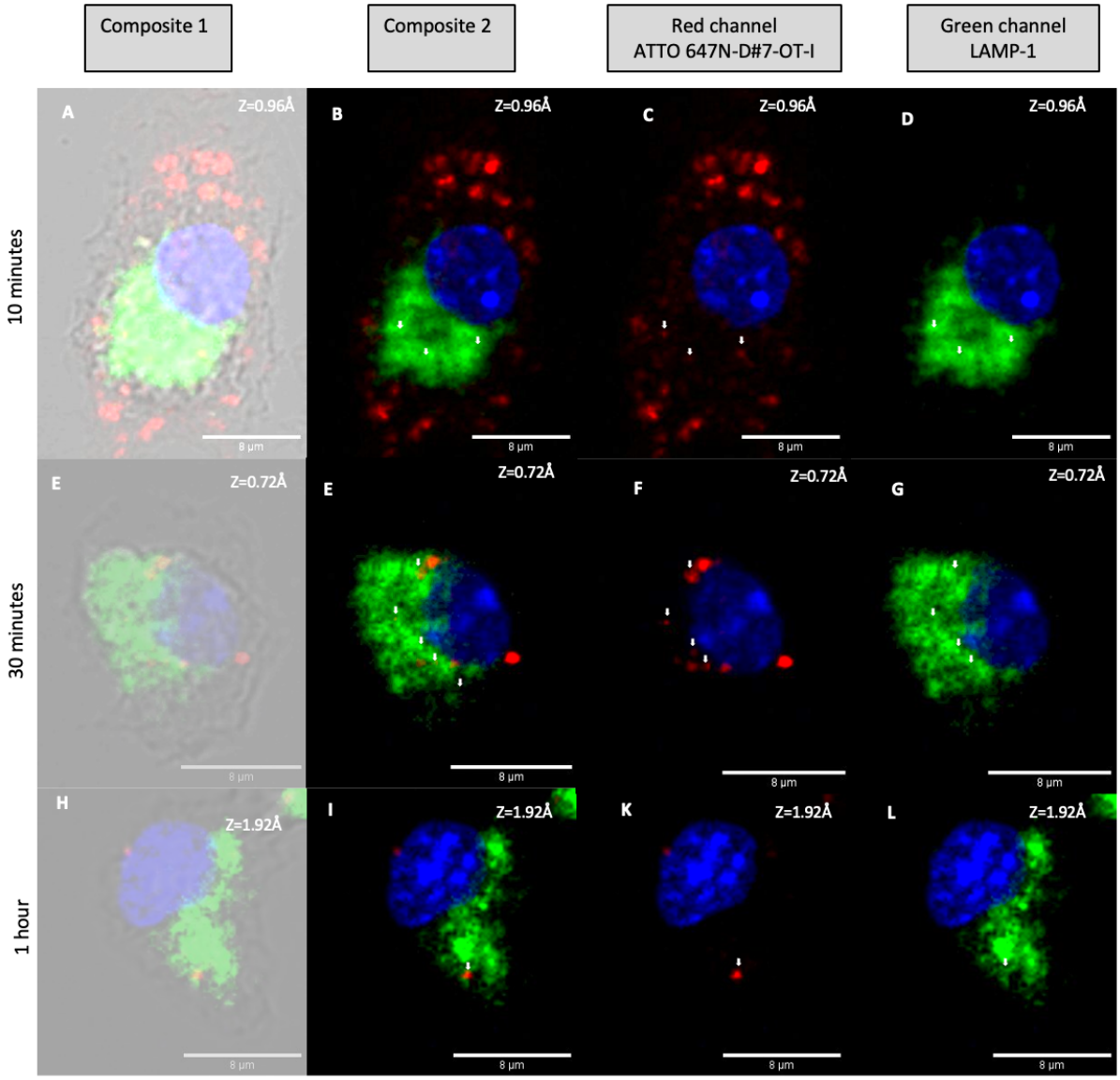

Figure 6: Immunostaining of DCs internalized with ATTO 647N-D#7-OT-I (red signals) at three timepoints and Alexa Fluor 488 (green signals) to label LAMP-1 on lysosomes. The picture depicts three timepoints at 10 minutes, 30 minutes and 1 hour. Composite 1 comprises all channels with bright field showing the borders of the cells. Composite 2 excludes bright field, illustrating the green and red channels together. DAPI (blue) indicates the nucleus of the cell. Possible colocalizations between ATTO 647N and Alexa Fluor 488 are marked by white arrows in Composite 2, Red and Green channels. Each image is performed with a scale bar (8µm) and Z stack (Å). (A) Bright field at 10 minutes. (B) Composite at 10 minutes. (C) Red channel of ATTO 647N label at 10 minutes. (D) Green channel of Alexa488-anti-LAMP-1 at 10 minutes. (E) Bright field at 30 minutes. (F) Composite at 30 minutes. (G) Red channel of ATTO 647N label at 30 minutes. (H) Green channel of Alexa488-anti-LAMP-1 at 30 minutes. (I) Bright field at 1 hour. (J) Composite at 1 hour. (K) Red channel of ATTO 647N label at 1 hour. (L) Green channel of Alexa488-anti-LAMP-1 at 1 hour. The signals of ATTO 647N-labelled conjugates were very strong at 10 minutes but the correlation was still weak between the red and green channels. The red spots were significantly reduced over time. Alexa488-anti-LAMP-1 was obtained as clouds of green signals in the cells.

When compared with ATTO 647N-D#7-OT-I, ATTO 647N-D#7 was depicted in Figure 7 with a similar pattern of colocalization in the three organelles. There was possible colocalization in all three organelles at 10 minutes. The colocalization at later timepoint was the same between three cellular compartments. More importantly, the internalization of this free aptamer was checked for 2 hours (results not shown). However, the signals of ATTO 647N-D#7 mostly

disappeared in DCs at this timepoint. The signals were not significant enough for colocalization analysis with ImageJ.

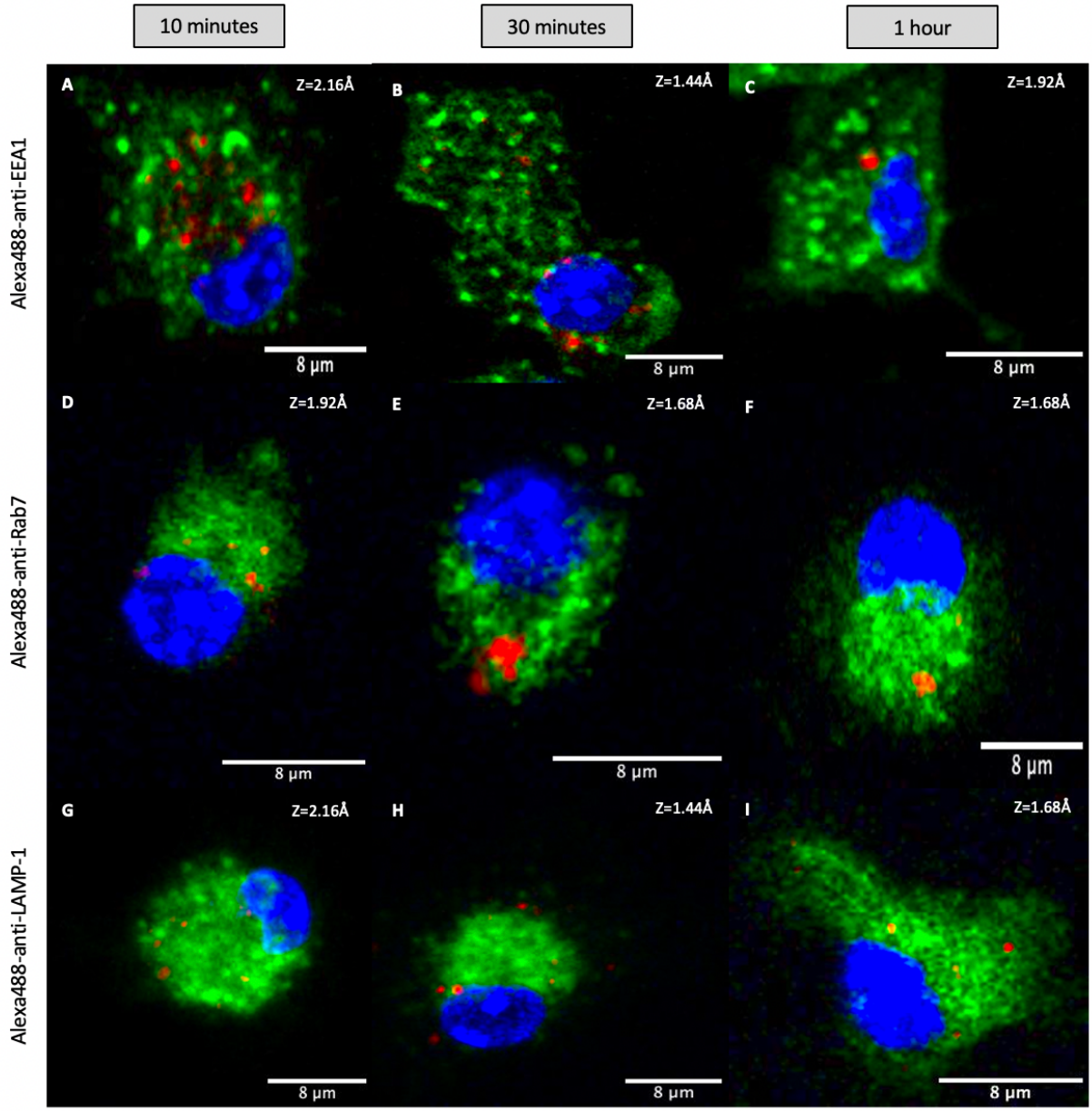

Figure 7: Immunostaining of DCs internalized with ATTO 647N-D#7 (red signals) at three timepoints and Alexa Fluor 488 (green signals) to label the organelles inside DCs. The picture depicts three timepoints at 10 minutes, 30 minutes and 1 hour. Alexa488-anti-EEA1 marks early endosomes while Alexa488-anti-Rab7 recognizes late endosomes. Alexa488-anti-LAMP-1 labels lysosomes. DAPI (blue) labels the nucleus of the cell. Each image is shown in composite consisting of all channels at a specific time point, a scale bar (8µm) and Z stack (Å). (A) Cell labelled with Alexa488-anti-EEA1 after 10 minutes of internalization. (B) Cell labelled with Alexa488-anti-EEA1 after 30 minutes of internalization. (C) Cell labelled with Alexa488-anti-EEA1 after 1 hour of internalization. (D) Cell labelled with Alexa488-anti-Rab7 after 10 minutes of internalization. (E) Cell labelled with Alexa488-anti-Rab7 after 30 minutes of internalization. (F) Cell labelled with Alexa-anti-Rab7 after 1 hour of internalization. (G) Cell labelled with Alexa488-anti-LAMP-1 after 10 minutes of internalization. (H) Cell labelled with Alexa488-anti-LAMP-1 after 30 minutes of internalization. (I) Cell labelled with Alexa488-anti-LAMP-1 after 1 hour of internalization. At 10 minutes, the signals of ATTO 647N-D#7-OT-Isc were stronger than after 30 minutes and 1 hour. There were possible colocalizations of the conjugates inside early endosomes, late endosomes and lysosomes at three timepoints although they were most significant at 10 minutes.

4.3. Kinetics study

During the kinetics study, the data of ATTO 647N-labelled D#7, D#7-OT-I and D#7-OT-Isc were used for the calculation of PCC to determine the correlation of these conjugates with three

organelles at 10 minutes, 30 minutes and 1 hour. The averages and standard deviations were obtained to perform and compare these groups of samples in graphs (Figure 8). During the experiments, the colocalization of ATTO 647N-D#7-OT-Isc in early endosomes at 1 hour and in late endosomes at 10 minutes failed to be collected.

In general, the colocalization of the conjugates with all three investigated cellular compartments decreased gradually. The standard deviations of the data were quite high. In addition, there was a weak correlation between the conjugates and the early endosomes at 10 minutes (PCC > 0.4). Noticeably, the colocalization of two conjugates in early endosomes were higher than the colocalization in late endosomes and lysosomes at the same time (PCC≈ 0.3). However, at 30 minutes, the differences in colocalization with three organelles were not at all significant, ranging from 0.12 to 0.17 in all three organelles (Figure 8).

Meanwhile, the free aptamer ATTO 647N-D#7 showed a different route from the conjugates. The correlation in three organelles at 10 minutes were significantly lower, especially in early endosomes (graph A, D and G in Figure 8). Importantly, the colocalization in early endosomes and lysosomes maintained almost the same or became slightly lower at 30 minutes when compared with the colocalization at 10 minutes (graph A in Figure 8).

To check if OT-I influenced the destination of the aptamers, statistical analysis was performed to compare between ATTO 647N-D#7 and ATTO 647N-D#7-OT-I. The significant difference was found for the colocalization of the free aptamer in early endosomes over three timepoints. Additionally, the colocalization was also significantly different in late endosomes and lysosomes at 30 minutes (p-value < 0.05). The PCC averages of ATTO 647N-D#7 in these organelles at the mentioned timepoints were greater than ATTO 647N-D#7-OT-I.

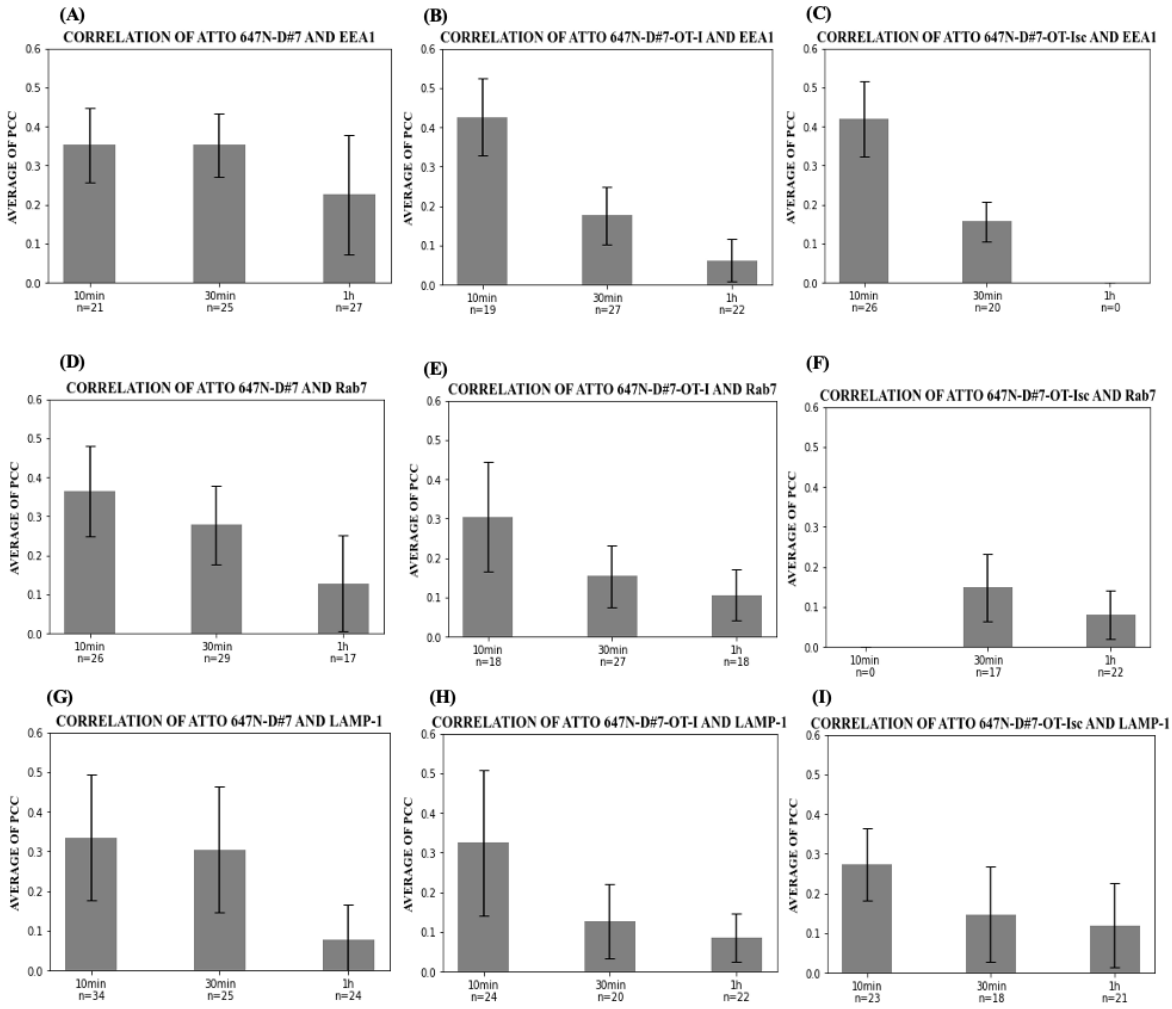

Figure 8: Bar graph of the kinetics study at three timepoints (10 minutes, 30 minutes and 1 hour) performing the colocalization of the free aptamers or the conjugates and cellular organelles. The graph shows the averages of PCC over time with error bars indicating standard deviations and the number of sample size (n) for each experimental group. (A) The correlation between ATTO 647N-D#7 and early endosome labelled with EEA1. (B) The correlation between ATTO 647N-D#7-OT-I and early endosomes labelled with EEA1. (C) The correlation between ATTO 647N-D#7-OT-Isc and early endosomes labelled with EEA1. (D) The correlation between ATTO-D#7 and late endosomes labelled with Rab7. (E) The correlation between ATTO 647N-D#7-OT-I and late endosomes labelled with Rab7. (F) The correlation between ATTO-D#7-OT-Isc and early endosomes labelled with Rab7. (G) The correlation between ATTO 647N-D#7 and lysosomes labelled with LAMP-1. (H) The correlation between ATTO 647N-D#7-OT-I and lysosomes labelled with LAMP-1. (I) The correlation between ATTO 647N-D#7-Isc and lysosomes labelled with LAMP-1. The averages of PCC have the tendency to decrease over time between the conjugates and the cellular organelles. There was weak correlation between the conjugates with all three organelles at 10 minutes, especially with early endosomes. The averages of PCC were close to 0.5 for the colocalization of the conjugates in the early endosomes marked by EEA1. Meanwhile, these values were less than 0.4 for the conjugates in other organelles. For ATTO 647N-D#7, the correlation at 10 minutes was even weaker, which was less than 0.4 in early endosomes, late endosomes and lysosomes. Furthermore, colocalization between the free aptamers and EEA-1 on early endosomes did not decrease from 10 to 30 minutes.

To examine if OT-I lead to a specific pathway to process the conjugates, p-value < 0.05 was used to check statistical significance between ATTO 647N-D#7-OT-I and ATTO 647N-D#7-OT-Isc. There was no significant difference in the colocalization of the two conjugates with the three cellular organelles including early endosomes, late endosomes and lysosomes (results not shown).

Importantly, Table 3 shows the statistical analysis to compare the colocalization of ATTO 647N-D#7-OT-I in early endosomes with the other two cellular compartments. Hence, the route of this conjugate could be revealed.

Table 3: p-value between the colocalization of ATTO-D#7-OT-I in early endosomes with other organelles at a specific timepoint.

Organelle 1	Organelle 2	Time	p-value	Statistical significance (p-value<0.05)*
EEA1-early endosome	Rab7-late endosome	10 minutes	0.002	Significantly greater
EEA1-early endosome	LAMP-1-lysosome	10 minutes	0.013	Significantly greater
EEA1-early endosome	Rab7-late endosome	30 minutes	0.143	No difference
EEA1-early endosome	LAMP-1-lysosome	30 minutes	0.030	Significantly greater
EEA1-early endosome	Rab7-late endosome	1 hour	0.014	Significantly lower
EEA1-early endosome	LAMP-1-lysosome	1 hour	0.114	No difference

***** The statistical significance was set at p-value < 0.05. When p > 0.05, there was no significant difference between two experimental groups. When p < 0.05, the colocalization of the aptamers with EEA1-early endosomes was either significantly greater or lower than the colocalization in the other organelle, depending on the tail of the statistical test.

Table 4: p-value between the colocalization of ATTO-D#7 in early endosomes with other organelles at a specific timepoint.

Organelle 1	Organelle 2	Time	p-value	Statistical significance (p-value<0.05)*
EEA1-early endosome	Rab7-late endosome	10 minutes	0.346	No difference
EEA1-early endosome	LAMP-1-lysosome	10 minutes	0.315	No difference
EEA1-early endosome	Rab7-late endosome	30 minutes	0.002	Significantly greater
EEA1-early endosome	LAMP-1-lysosome	30 minutes	0.092	No difference
EEA1-early endosome	Rab7-late endosome	1 hour	7.9E-5	Significantly greater
EEA1-early endosome	LAMP-1-lysosome	1 hour	0.023	Significantly greater

* The statistical significance was set at p-value < 0.05. When p > 0.05, there was no significant difference between two experimental groups. When p < 0.05, the colocalization of the aptamers with EEA1-early endosomes was either significantly greater or lower than the colocalization in the other organelle, depending on the tail of the statistical test.

As a summary, there was a decrease in colocalization of ATTO 647N-D#7-OT-I with all three organelles from 10 minutes to 1 hour. After 10 minutes, the conjugates showed more significant colocalization in early endosomes than late endosomes and lysosomes. Notably, this statistical significance shifted gradually to show more colocalization with Rab7 on late endosomes after 1 hour. Meanwhile, the colocalization in LAMP-1 remained the lowest among the three organelles from 10 minutes to 1 hour (Table 3).

To check the possible location of ATTO 647N-D#7, the comparison between the colocalization in early endosomes and other organelles was also statistically analyzed, as shown in Table 4. Noticeably, ATTO 647N-D#7 showed a different route from ATTO 647N-D#7-OT-I. There was no significant difference between the three organelles at 10 minutes. Meanwhile, the colocalization in early endosomes was statistically more than the colocalization in late endosomes at 30 minutes. Furthermore, ATTO 647N-D#7 also tended to locate in early endosomes more than the other two organelles at 1 hour.

5. Discussion and conclusion

Regarding the immunostainings of DCs, this research was successful to determine the location of the aptamers and conjugates inside three cellular compartments including early endosomes, late endosomes, and lysosomes. As reported in the results, the green channels had many background signals due to autofluorescence and noise from the non-specific binding of secondary antibodies. Hence, clearing the noise in the staining was very essential for later colocalization analysis. Importantly, Alexa488-anti-EEA1 on early endosomes was seen as granular vesicles, which were easy to identify and differentiate from the background signals. Meanwhile, the signals given by Alexa488-anti-Rab7 on late endosomes and Alexa488-anti-LAMP-1 on lysosomes were more like clouds, which made it more difficult to discriminate between the specific signals and noise. By thresholding in ImageJ, the specific signals were identified to clear the noise, supporting later colocalization analysis. Consequently, the problems of autofluorescence and non-specific binding of the secondary antibodies were solved. Although the possible colocalization could be determined visually in the immunostainings, it is more reliable to use analytical statistics for this research because the colocalization should be scanned through all the Z-stacks in the cells. Hence, it avoids

spontaneous colocalization in a random plane of DCs. Moreover, visual identification could be misleading when the green signals are more powerful than the red signals or vice versa. Therefore, missing out colocalization information might happen.

Importantly, the new protocol was able to analyze the colocalization of the free aptamers and conjugates over time inside DCs. The kinetics study managed to reveal the routes of these molecules in the cells. As expected, the pathways of D#7-OT-I and D#7 were completely distinct.

Regarding the colocalization of D#7-OT-I, the conjugates tended to stay predominantly inside early endosomes at 10 minutes. However, the location of this conjugate shifted gradually to late endosomes at later timepoints. This result was comparable to the experimental set-up of the internalization of red-dye latex beads (LB) inside antigen-presenting cells done by Sophie Duclos *et al*.[22]. The experiments were designed to internalize LB for 15 minutes to detect early endosomes and 60 minutes to identify late endosomes/lysosomes. Hence, this comparison could confirm the reliability of the results in this research. Remarkably, D#7-OT-I not only involved early endosomes to activate cytotoxic T cells but also participated in the pathway initiating presenting antigens to MHC class II. The reasons for this fact could vary.

First, as mentioned above, the purification step of the conjugates showed a sign of fragmented peptides. Hence, it is questionable whether the conjugated peptides in the produced molecules were actual OT-I or just a small sequence of OT-I. When looking at the results between D#7-OT-I and D#7-OT-Isc, there was unexpectedly no statistical difference (p-value > 0.05) in the shown data as seen in Figure 8. This possibly indicates no differences between OT-I and OT-Isc due to the fragmentation.

Secondly, empirical research also proved that specific receptors such as CD40 or MR initiate cross-presentation on MHC class I more efficiently than some others such as DEC205 [23]. As mentioned above, DEC205 receptor is mainly responsible for the pathway presenting antigens on MHC class II, activating $CD4^+$ T cells. In fact, according to Bithi Chatterjee *et al.*[23], antigens binding to DEC205 *in vitro* also showed cross-presentation to modulate the maturation of cytotoxic T cells with significantly lower efficiency than the specialized receptors including MR. Therefore, a small number of the antigens, D#7-OT-I were possibly processed within late endosomes and lysosomes in addition to the specialized pathway for cross-presentation on MHC class I. As stated in the research of Dr. Haßel, the conjugate of D#7 and OT-II, a small sequence of OVA protein with specific binding regions of MHC class II, could promote the activities of $CD4^+$ T cells [11]. Consequently, by comparing with the previous studies, the result of this research highlights the fact that D#7-OT-I was possibly processed in the two pathways of antigen presentation on MHC molecules. However, processing inside early endosomes and cytosols tended to be more predominant. More importantly, Lillian Cohn *et al.* [24] reported that the conjugates can possibly escape the lysosomal activities depending on the cell types. Therefore, there are many possibilities that the conjugates of D#7 and OT-I can still lead to the activation of cytotoxic T cells even when they were translocated to late endosomes/lysosomes.

As a summary, the conclusion could be drawn to unlock the pathway of D#7 inside DCs. At 10 minutes, the free aptamers without the peptides located in all three organelles such as early endosomes, late endosomes and lysosomes with the same amount. After the breakdown, the remaining signals stayed predominantly inside early endosomes. The degradation of the free aptamers probably occurred due to the activities of the enzymes inside cytosols and lysosomes. At 2 hours, the signals of D#7 were significantly weak and unclear, indicating the degradation of either the aptamers or the breakdown of only ATTO 647N. Although the route of D#7 was different from D#7-OT-I, it makes sense when compared with the previous study. As discussed above, the conjugation of D#7 and OT-II enabled the activation of T helper cells via antigen

presenting on MHC-class II, according to the research of Dr. Haßel [11]. Therefore, D#7 might participate in two pathways with the same possibility by binding to multiple receptors specific to DCs. These receptors might lead to two processing pathways, presenting antigens on both MHC class I and II. Remarkably, the antigens transported by the aptamers could impact the route and the processing of conjugates inside DCs, making them more specialized for antigen presentation to a specific group of T cells later on.

More importantly, it should be considered that the pathway in this research centered ATTO-D#7, not the antigens. The peptides themselves possibly influenced the movement of the conjugates but it does not mean that OT-I had exactly the same route as D#7. At some points along the way, the peptides might be cleaved off from the conjugates and processed differently from D#7. An observation of fluorophore-conjugated OT-I peptides in DCs can be exploited to compare with the conjugate and aptamer pathways. Besides, the experiments need to be repeated to confirm the reliability of the results.

Regarding the reliability of the method of colocalization analysis by ImageJ software, there are also some remarks. As can be seen in Appendix 1, this method used a whole cell for the data analysis because the signals of aptamers were scattered and small, which were difficult to threshold automatically by coding. It is very easy to reject the significant signals of the red channels at the later timepoints because ATTO 647N signals were very weak at this time after major degradation. Consequently, selecting the regions of only the red signals was more difficult. However, choosing a whole cell as the region of interest for colocalization analysis has drawback. PCC was chosen as the algorithm to analyze colocalization in this thesis, which reflects the linear correlation between two signals. When it is close to 1, it means the intensities of the two signals proportionally increase or decrease in one pixel [19]. Hence, PCC reflects if two signals correlate in a linear relationship or not. Meanwhile, it is not the case for internalization experiments [19]. Because not all the vesicles labelled by green signals contained aptamers, PCC was reduced although there was a high rate of colocalization between the two signals. Furthermore, the signals given by the markers on cellular organelles were not proportional with the aptamers internalized into the vesicles. The red signals were dependent on the concentration of the internalized aptamers while the green intensity depended on the distribution of this marker on the membrane such as EEA1 on early endosomes. Therefore, the intensities of the two signals were not correlated. These reasons can reduce the actual statistics of colocalization by PCC. Apart from these disadvantages, PCC has an advantage over other commonly used method such as Mander's correlation coefficient. PCC method is less affected by noise so that the threshold procedure is more simple and straightforward [19].

In general, the standard deviations were very considerable, especially in lysosomes (Figure 8). Because the uptake rate of the cells can vary and the speed of aptamer movements might slightly differ between cells, PCC numbers can range widely. Furthermore, as described above, the staining of Alexa488-anti-LAMP-1 was obtained as clouds of green signals, which were not as clear as granular shapes of EEA1 on early endosomes. The quality of the staining made the results of colocalization in lysosomes more various because it had more random errors. It is possible that the colocalization just happened by chance due to the broad cloud shapes although in fact, there was no colocalization. Hence, the standard deviations ranged widely for the colocalization in lysosomes. Consequently, this method of colocalization analysis should be coupled with statistical analysis to unveil the kinetics of D#7 and D#7-OT-I.

According to the results of this research, it is interesting to know exactly when the conjugates were released to the cytosol and whether the peptides were cleaved off from the conjugates to undergo a separate process from the aptamers. This aim can be achieved by coupling the aptamers to a different antigen. For example, saporin was exploited for cytoplasmic delivery

of aptamers because saporin induces cytotoxicity once released in the cytosol by binding to and inhibiting ribosomes [25]. Once fully understanding this mechanism, D#7 can be certainly applied to generate vaccines against cancer cells and virus-infected cells since this aptamer had a capacity of presenting the antigens on MHC class I. Furthermore, D#7 is very versatile in such a way that it also undergoes processing in late endosomes/lysosomes. Hence, D#7 might contribute to a potent protein-based vaccine against virus such as Human Immunodeficiency Virus (HIV). According to the research of Barbara J. Flynn *et al*.[26], HIV Gag p24 transported by 3G9 antibody targeting DEC205 receptors of DCs induced the activation of both $CD4^+$ and $CD8^+$ T cells. Therefore, it is also interesting to investigate if D#7 as the transporter can modulate stronger immune responses and long-term immunity without a booster vaccination in the future.

Before starting new research, some problems should be solved in this study. To generate the conjugates of interest, maleimide-thiol coupling reaction was done to form three conjugates including ctrl-OT-I as the non-binding control, D#7-OT-I and D#7-OT-Isc as the experimental samples. The yield was generally low when compared with the previous study. According to the research of Dr. Haßel, maleimide-thiol coupling reactions could reach 34-56% [11]. Meanwhile, the highest yield in this study was only 26.77%. As reported by Chiara Da Pieve *et al.* [27], in the optimal conditions and optimized protocol, the yield can be as high as 80% when coupling the aptamers with polyethylene glycol (PEG). Additionally, the chromatogram illustrates many ghost peaks before 7 minutes and after 17 minutes, indicating contaminants in the column. The conjugates were difficult to be dissolved in DPBS, which was unexpected. It is possible to have some contaminants from the column and they were eluted in the collected samples. However, the contaminants were removed by Amicon 10K columns, leading to the solubility of the aptamers in a small volume of DPBS afterwards. In addition, there were multiple peaks at around 10 minutes, indicating fragmented peptides. This problem also resulted in the low yield of conjugates of interest. It is suggested to check the products with liquid chromatography-mass spectrometry (LC-MS) to determine whether the obtained conjugates were the desired products without the free aptamers and eluted unreactive peptides.

Additionally, there were some cells internalizing ctrl-OT-I and ctrl although ctrl aptamer does not have high affinity to DCs. The binding capacity of ctrl was determined by binding assays using flow cytometry in the research of Dr. Haßel [11]. The unexpected internalization can be explained by the fact that some molecules and substances are possibly taken up by non-specific phagocytosis. As expected, ctrl was internalized in DCs much less than D#7. Moreover, ctrl was taken up even less than ctrl-OT-I. This could be because the conjugation of the aptamers with OT-I might more or less change the conformation of ctrl, allowing more conjugates to be internalized [28]. Another reason is that OT-I might help to direct more internalization of the conjugates by receptor-mediated endocytosis. The research of Dr. Haßel showed that the incubation of DCs with OT-I alone could modulate the proliferation of $CD8^+$ T cells at high concentrations but the efficiency was much less than the induction by the conjugates [11].

In conclusion, this research was successful to identify the pathway of D#7 and D#7-OT-I inside DCs. Expectedly, the routes were completely different. Although there were some limitations due to the unexpected results, peptides certainly influenced the internalization and processing of the conjugates in DCs. Because D#7 was shown to participate in both pathways of antigen presentation, it holds great potential for future application in cancer research and vaccine development to target DCs, modulating the maturation of specific groups of T cells. As indicated in the introduction, D#7 was found to bind selectively to DCs, not B cells or T cells. Hence, utilizing D#7 possibly minimizes off-target effects, boosting the potency of the vaccines. Besides, understanding the pathway of D#7 inside DCs helps manipulate this transporter by conjugating it to a desired antigen in the future. Additionally, the newly

established protocol to analyze the colocalization of aptamers inside DCs was discussed in detail for the advantages and drawbacks. This protocol can be applied in similar study, which might need further optimization depending on the research purpose.

6. References

1. Stoltenburg, R., Reinemann, C., & Strehlitz, B. (2007). SELEX: A (r)evolutionary Method to Generate High Affinity Nucleic Acid Ligands. *Biomolecular Engineering*, *24*, 381–403. https://doi.org/10.1016/j.bioeng.2007.06.001

2. Keefe, A. D., Pai, S., & Ellington, A. (2010). Aptamers as therapeutics. *Nature Reviews Drug Discovery*, *9*(7), 537–550. https://doi.org/10.1038/nrd3141

3. Marshall, M. L., & Wagstaff, K. M. (2020). Internalized Functional DNA Aptamers as Alternative Cancer Therapies. *Frontiers in Pharmacology*, *11*. https://www.frontiersin.org/article/10.3389/fphar.2020.01115

4. Pendergrast, P. S., Marsh, H. N., Grate, D., Healy, J. M., & Stanton, M. (2005). Nucleic acid aptamers for target validation and therapeutic applications. *Journal of Biomolecular Techniques: JBT*, *16*(3), 224–234.

5. Zou, X., Wu, J., Gu, J., Shen, L., & Mao, L. (2019). Application of Aptamers in Virus Detection and Antiviral Therapy. *Frontiers in Microbiology*, *10*. https://www.frontiersin.org/article/10.3389/fmicb.2019.01462

6. Lakhin, A. V., Tarantul, V. Z., & Gening, L. V. (2013). Aptamers: Problems, Solutions and Prospects. *Acta Naturae*, *5*(4), 34–43.

7. Yoon, S., & Rossi, J. J. (2018). Aptamers: Uptake mechanisms and intracellular applications. *Advanced Drug Delivery Reviews*, *134*, 22–35. https://doi.org/10.1016/j.addr.2018.07.003

8. Patente, T. A., Pinho, M. P., Oliveira, A. A., Evangelista, G. C. M., Bergami-Santos, P. C., & Barbuto, J. A. M. (2019). Human Dendritic Cells: Their Heterogeneity and Clinical Application Potential in Cancer Immunotherapy. *Frontiers in Immunology*, *9*. https://www.frontiersin.org/article/10.3389/fimmu.2018.03176

9. Muñoz Wolf, N., & Lavelle, E. (2018). A Guide to IL-1 family cytokines in adjuvanticity. *The FEBS Journal*, *285*. https://doi.org/10.1111/febs.14467

10. Zablon, F. M. (2021, April 21). *MHC Molecules, Antigen Processing and Presentation*. The Biology Notes. https://thebiologynotes.com/mhc-molecules-antigen-processing-presentation/

11. Haßel, S. K. (2016). *Aptamers for targeted activation of T cell-mediated immunity*. *Dissertation zur Erlangung des Doktorgrades (Dr. rer. nat.) der Mathematisch-Naturwissenschaftlichen Fakultät der Rheinischen Friedrich-Wilhelms-Universität Bonn*, 134.

12. Roche, P. A., & Furuta, K. (2015). The ins and outs of MHC class II-mediated antigen processing and presentation. *Nature Reviews Immunology*, *15*(4), 203–216. https://doi.org/10.1038/nri3818

13. Khan, N., Chen, X., & Geiger, J. D. (2020). Role of Endolysosomes in Severe Acute Respiratory Syndrome Coronavirus-2 Infection and Coronavirus Disease 2019 Pathogenesis: Implications for Potential Treatments. *Frontiers in Pharmacology*, *11*. https://www.frontiersin.org/article/10.3389/fphar.2020.595888

14. Trausch, J. J., Shank-Retzlaff, M., & Verch, T. (2017). Replacing antibodies with modified DNA aptamers in vaccine potency assays. *Vaccine*, *35*(41), 5495–5502. https://doi.org/10.1016/j.vaccine.2017.04.003

15. Wengerter, B., Katakowski, J., Rosenberg, J., Park, C., Almo, S., Palliser, D., & Levy, M. (2014). Aptamer-Targeted Antigen Delivery. *Molecular Therapy : The Journal of the American Society of Gene Therapy*, *22*. https://doi.org/10.1038/mt.2014.51

16. Wilson, J. M., de Hoop, M., Zorzi, N., Toh, B.-H., Dotti, C. G., & Parton, R. G. (2000). EEA1, a Tethering Protein of the Early Sorting Endosome, Shows a Polarized Distribution in Hippocampal Neurons, Epithelial Cells, and Fibroblasts. *Molecular Biology of the Cell*, *11*(8), 2657–2671.

17. Eskelinen, E.-L. (2006). Roles of LAMP-1 and LAMP-2 in lysosome biogenesis and autophagy. *Molecular Aspects of Medicine*, *27*(5–6), 495–502. https://doi.org/10.1016/j.mam.2006.08.005

18. Zhang, M., Chen, L., Wang, S., & Wang, T. (2009). Rab7: Roles in membrane trafficking and disease. *Bioscience Reports*, *29*(3), 193–209. https://doi.org/10.1042/BSR20090032

19. Dunn, K. W., Kamocka, M. M., & McDonald, J. H. (2011). A practical guide to evaluating colocalization in biological microscopy. *American Journal of Physiology. Cell Physiology*, *300*(4), C723-742. https://doi.org/10.1152/ajpcell.00462.2010

20. *Bridging the gap between qualitative and quantitative colocalization results in fluorescence microscopy studies | Scientific Reports*. (n.d.). Retrieved 3 July 2022, from https://www.nature.com/articles/srep01365

21. *Wilk Test—An overview | ScienceDirect Topics*. (n.d.). Retrieved 31 May 2022, from https://www.sciencedirect.com/topics/mathematics/wilk-test

22. Duclos, S., Clavarino, G., Rousserie, G., Goyette, G., Boulais, J., Camossetto, V., Gatti, E., LaBoissière, S., Pierre, P., & Desjardins, M. (2011). The endosomal proteome of macrophage and dendritic cells. *PROTEOMICS*, *11*(5), 854–864. https://doi.org/10.1002/pmic.201000577

23. Chatterjee, B., Smed-Sörensen, A., Cohn, L., Chalouni, C., Vandlen, R., Lee, B.-C., Widger, J., Keler, T., Delamarre, L., & Mellman, I. (2012). Internalization and endosomal degradation of receptor-bound antigens regulate the efficiency of cross presentation by human dendritic cells. *Blood*, *120*(10), 2011–2020. https://doi.org/10.1182/blood-2012-01-402370

24. Cohn, L., Chatterjee, B., Esselborn, F., Smed-Sörensen, A., Nakamura, N., Chalouni, C., Lee, B.-C., Vandlen, R., Keler, T., Lauer, P., Brockstedt, D., Mellman, I., & Delamarre, L. (2013). Antigen delivery to early endosomes eliminates the superiority of human blood BDCA3+ dendritic cells at cross presentation. *The Journal of Experimental Medicine*, *210*(5), 1049–1063. https://doi.org/10.1084/jem.20121251

25. Dickey, D. D., Dassie, J. P., & Giangrande, P. H. (2016). Method for Confirming Cytoplasmic Delivery of RNA Aptamers. *Methods in Molecular Biology (Clifton, N.J.)*, *1364*, 209–217. https://doi.org/10.1007/978-1-4939-3112-5_17

26. Flynn, B. J., Kastenmüller, K., Wille-Reece, U., Tomaras, G. D., Alam, M., Lindsay, R. W., Salazar, A. M., Perdiguero, B., Gomez, C. E., Wagner, R., Esteban, M., Park, C. G., Trumpfheller, C., Keler, T., Pantaleo, G., Steinman, R. M., & Seder, R. (2011). Immunization with HIV Gag targeted to dendritic cells followed by recombinant New York vaccinia virus induces robust T-cell immunity in nonhuman primates. *Proceedings of the National Academy of Sciences of the United States of America*, *108*(17), 7131–7136. https://doi.org/10.1073/pnas.1103869108

27. Da Pieve, C., Williams, P., Haddleton, D. M., Palmer, R. M. J., & Missailidis, S. (2010). Modification of Thiol Functionalized Aptamers by Conjugation of Synthetic Polymers. *Bioconjugate Chemistry*, *21*(1), 169–174. https://doi.org/10.1021/bc900397s

28. Elskens, J. P., Elskens, J. M., & Madder, A. (2020). Chemical Modification of Aptamers for Increased Binding Affinity in Diagnostic Applications: Current Status and Future Prospects. *International Journal of Molecular Sciences*, *21*(12), 4522. https://doi.org/10.3390/ijms21124522

29. *Clearing background in a Z-Stack—Image Analysis*. (2020, June 8). Image.Sc Forum. https://forum.image.sc/t/clearing-background-in-a-z-stack/35864/14

30. *Pearson's Correlation Coefficient*. (n.d.). Statistics Solutions. Retrieved 17 June 2022, from https://www.statisticssolutions.com/free-resources/directory-of-statistical-analyses/pearsons-correlation-coefficient/

Appendix 1

After immunostaining was done, the images were checked by LSM. The images included multiple channels such as bright field, DAPI signals of the nucleus, red channels of conjugate signals and green channels of the organelles. Colocalization analysis was done for each cell separately. Hence, the selection of individual cells was done manually by Crop tools provided by ImageJ. In addition, only the Z-stack with the signals of the conjugates were included for analysis. When importing the images into ImageJ, the image was split into separate channels. The red signals were not intrinsic in the cells and there was not much noise in the red channel (Figure 9,10 and 11). Besides, the signals of the conjugates became very weak after long time of internalization. Excluding the noise and too much image processing could risk missing out the signals of interest. However, the green signals of Alexa Fluor 488 had significant noise. Additionally, the green signals were intrinsic in the cells (autofluorescence). A faint signal of green color could be found in the negative controls, cells with only DAPI and cells without primary antibodies as mentioned in the Materials and Methods section. Because there was much background in the immunostaining images of the green channels, excluding noise was essential. Threshold was used to create a mask and delete the non-specific signals outside the mask [29]. There were sixteen methods of Auto threshold provided by ImageJ. Different methods were used for distinct organelles, depending on the patterns of the cellular compartments and the quality of the immunostaining. Moments method was used as Auto threshold of Alexa488-anti-EEA1 and Alexa488-anti-Rab7 (Figure 9 and 10). Meanwhile, RenyiEntropy method was chosen as Auto threshold for Alexa488-anti-LAMP-1 (Figure 11). Despeckle tool was chosen after thresholding to exclude some small dots and trivial signals created by the Auto threshold.

Importantly, the signals of Alexa Fluor 488 on the same cellular compartments could be unevenly distributed throughout the cells, depending on the distribution of the markers and the chosen Z-stack. Hence, making the signals more even is very essential because it significantly affects the results of PCC [19]. To achieve this aim, Filter was used to sharpen and smoothen the signals within the cells. Median mode of 1 radius was utilized as a Filter method for all three cellular compartments. After modifying the images, red channels and green channels were chosen as the input in JACoP plugin. The colocalization was analyzed in all Z-stack. Therefore, the input should have the same depth (number of Z-stack) and the same size (number of pixels).

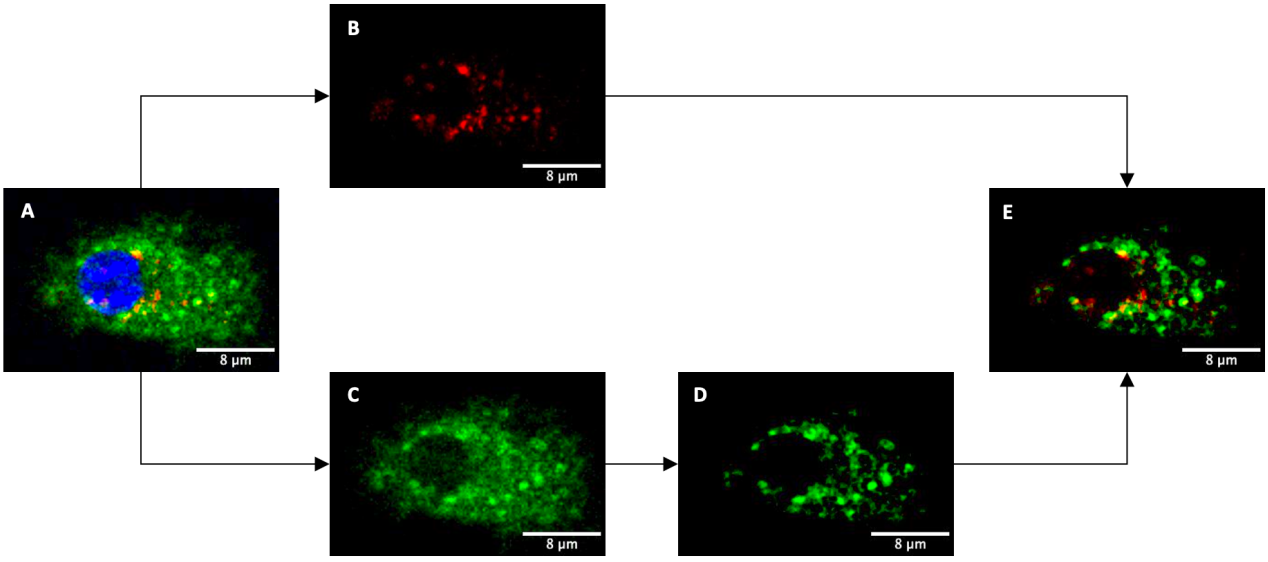

Figure 9: Image processing of cells internalized with conjugates and staining of early endosomes (Alexa488-anti-EEA1). Each image is labelled with a scale bar of 8µm. The image was split into red channel (ATTO 647N-labelled

conjugates) and green channel (Alexa488-anti-EEA1). The image was processed to exclude noise by thresholding (Moments method) and filtering (Median, 1 radius). (A) Merged image of DAPI (nucleus), red channel (conjugates) and green channel (early endosomes). (B) Red channel of the image (ATTO 647N-labelled conjugates). (C) Green channel of the image (Alexa488-anti-EEA1-early endosomes). (D) Green channel of the image after processing. (E) Merged channel of red channel and processed green channel.

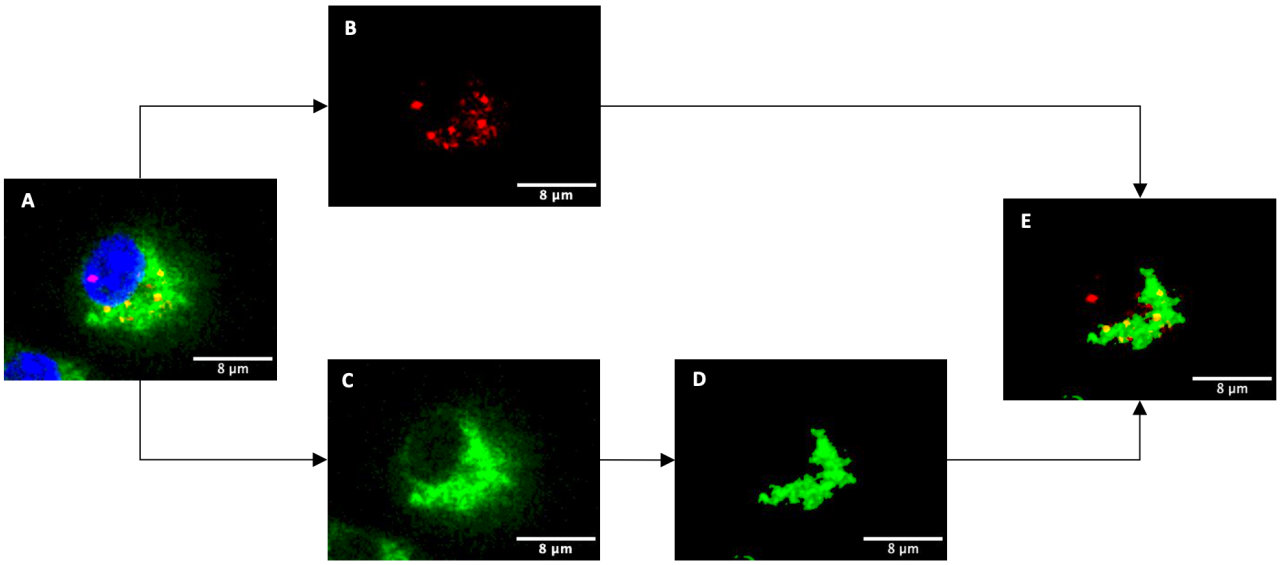

Figure 10: Image processing of cells internalized with conjugates and staining of lysosomes (Alexa488-anti-LAMP-1). Each image is labelled with a scale bar of 8µm. The image was split into red channel (ATTO 647N-labelled conjugates) and green channel (Alexa488-anti-Rab7). The image was processed to exclude noise by thresholding (RenyiEntropy method) and filtering (Median, 1 radius). (A) Merged image of DAPI (nucleus), red channel (conjugates) and green channel (lysosomes). (B) Red channel of the image (ATTO 647N-labelled conjugates). (C) Green channel of the image (Alexa488-anti-Rab7-lysosomes). (D) Green channel of the image after processing. (E) Merged channel of red channel and processed green channel.

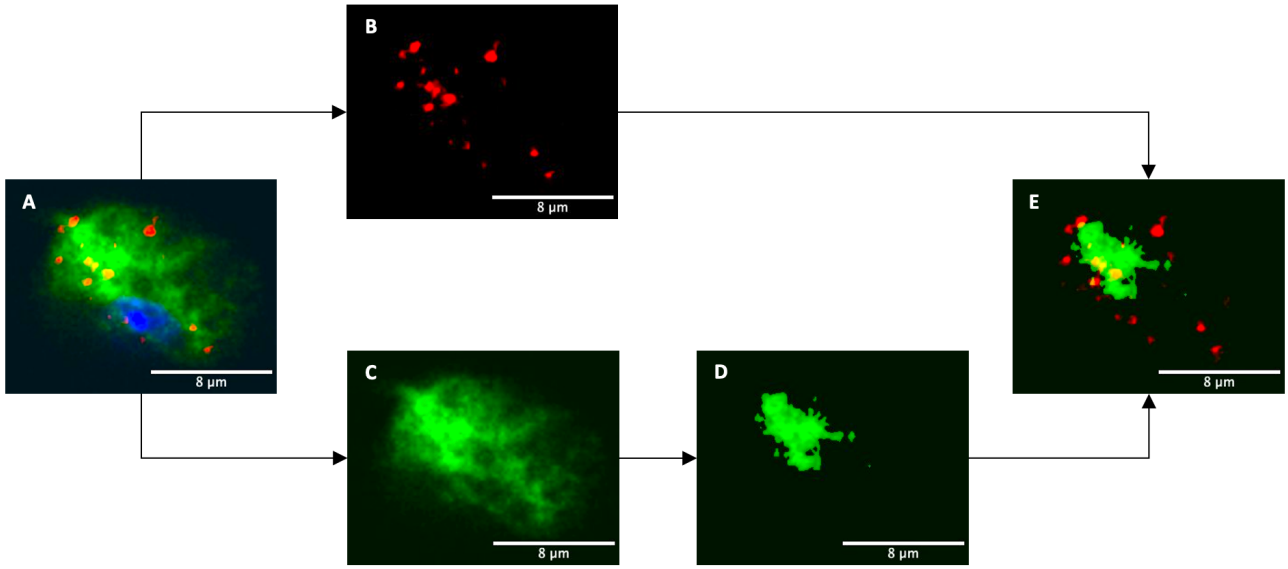

Figure 11: Image processing of cells internalized with conjugates and staining of lysosomes (Alexa488-anti-LAMP-1). Each image is labelled with a scale bar of 8µm. The image was split into red channel (ATTO 647N-labelled conjugates) and green channel (Alexa488-anti-EEA1). The image was processed to exclude noise by thresholding and filtering (Median, 1 radius). (A) Merged image of DAPI (nucleus), red channel (conjugates) and green channel (early endosomes). (B) Red channel of the image (ATTO 647N-labelled conjugates). (C) Green channel of the image (Alexa488-anti-EEA1-early endosomes). (D) Green channel of the image after processing. (E) Merged channel of red channel and processed green channel.

To automate similar procedure for all images, Macro coding written in IJ1 Macro language was used to open the images one by one (Appendix 2). PCC results were used to interpret the data

of correlation. There are negative correlations between two channels when one signal increases and the other signal decreases in intensities and vice versa ($0 > PCC > -1$). If $PCC = 0$, there are no correlations between two channels. There are positive correlations if PCC is greater than 0. However, $0<PCC<0.5$ only indicates a weak or moderate correlation while $0.5 < PCC < 1$ means the signals in two channels are strongly correlated in a linear relationship [30].

Appendix 2

1. Coding to open images in a large batch

This set of coding opens the images ending with ".tif" files in a folder and allows ImageJ to start processing images automatically one by one. Furthermore, the folder to save files at the end of the analysis is also chosen:

```
// Choose the folder to open
msga="Please choose the input folder";
waitForUser(msga);
dir1 = getDirectory("Choose Source Directory ");
list = getFileList(dir1);
// Choose the folder to save
msga="Please choose the output folder";
waitForUser(msga);
Output = getDirectory("Choose the output folder ");
// Each image ending with ".tif" is opened one by one
for (k = 0; k<list.length; k++) {
if (endsWith(list[k],".tif")){
showProgress(k+1, list.length);
open(dir1+list[k]);
}
}
```

2. Coding to eliminate noise and smoothen the images

This set of coding allows ImageJ to eliminate the noise in the images [29] and create filter in green channels. Therefore, the resulting green channels have less noise. The image processing was done for all Z stack:

```
// Retrieve the title of the image
title=getTitle();
// Split an image into multiple channels for further processing
run("Split Channels");
selectWindow("C4-"+ title);
close();
selectWindow("C2-"+ title);
close();
selectWindow("C3-"+title);
titleC3= "C3-"+title;
// Duplicate channel 3 (green) and rename to "threshold"[29]
run("Duplicate...","title=threshold duplicate");
run("Green");
selectWindow("threshold");
run("Auto Threshold","method=Moments ignore_dark white stack");
run("Despeckle", "stack");
// Create a mask to save threshold of all stacks in one image[29]
run("Analyze Particles...", "size=0-infinity show=Masks stack");
rename("Mask");
roiManager("reset");
selectWindow("Mask");
while (getSliceNumber()<nSlices){
run("Create Selection");
type = selectionType();
if (type==-1)
run("Next Slice [>]");
else
roiManager("Add");
run("Next Slice [>]");}
// Create selection to draw lines around the border of the mask[29]
```

```
run("Create Selection");
roiManager("Add");
selectWindow(titleC3);
rois = newArray();
// Overlay the selection of the mask on each stack of the image one by
one[29]
for(i=0;i<roiManager("count");i++){
   roiManager("Select",i);
// Clear the non-specific signals outside the selection
   run("Clear Outside","Slice");
// Add the processed stack into a new array of image[29]
   rois = Array.concat(rois,getSliceNumber());
}
Array.print(rois);
selectWindow(titleC3);
// Put Filter to smoothen the signals
run("Median...", "radius=1 stack");
selectWindow("C1-"+ title);
titleC1= "C1-"+title;
selectWindow("C1-"+title);
run("Red");
```

3. Input the images into JACoP plugin

This set of coding selects the chosen channels as the input in JACoP plugin. Pearson's correlation coefficient is chosen as the method to perform analysis. The final data is saved as a ".txt" file in the selected folder mentioned above:

```
// Importing the images into JACoP plugin
run("JACoP ", "imga=["+ titleC1 + "] imgb=[" + titleC3 + "] pearson");
run("Close All");
close("Roi Manager");
selectWindow("Log");
// Save the file as "Results.txt"
saveAs("Text", Output+"Results.txt")
close("Log");
```